

Scatterometer observations of wind variations induced by oceanic islands: Implications for wind-driven ocean circulation

Cédric Chavanne, Pierre Flament, Rick Lumpkin, Bénédicte Dousset, and Abderrahim Bentamy

Abstract. Scatterometer data at 25-km resolution are used to investigate the effects of the Hawaiian and Cabo Verde islands on the mean atmospheric flow. A wake of weak winds, flanked by accelerated winds, appears for each major island of both archipelagos. The resulting wind stress curl displays dipole-like structures, with positive values on the northern side and negative values on the southern side of the lee, extending several island diameters downwind. These curl anomalies reach a magnitude of $2 \cdot 10^{-6} \text{ Pa}\cdot\text{m}^{-1}$ and correspond to Ekman pumping velocities of $3 \text{ m}\cdot\text{day}^{-1}$ for Hawaii and $4 \text{ m}\cdot\text{day}^{-1}$ for Cabo Verde. They spin up cyclonic eddies on the north side and anticyclonic eddies on the south side of the lee of each island. The response of the ocean circulation is investigated using a simple Sverdrup balance. Two counter-rotating Sverdrup gyres are spun up west of the island of Hawaii and extend to the western boundary of the Pacific Ocean. They result in an eastward zonal transport confined between 19° and 20°N . East of 170°W , the surface expression of this transport coincides with the Hawaiian Lee Counter Current. Similar gyres are anticipated to form in the Atlantic Ocean, but remain to be observed. These results suggest that strong mesoscale patterns in the wind field occurring in the lee of high-topography features must be resolved to force global ocean circulation models.

Résumé. Des données diffusiométriques sont utilisées à une résolution de 25 km pour étudier les effets des îles d'Hawaii et du Cap Vert sur l'écoulement atmosphérique. Un sillage de vents faibles, bordé de vents accélérés, est associé à chaque île des deux archipels. Le rotationnel de la tension du vent a une structure dipolaire, avec des valeurs positives au nord et négatives au sud du sillage, s'étendant de plusieurs fois le diamètre de l'île sous le vent. Les anomalies de rotationnel atteignent une amplitude de $2 \cdot 10^{-6} \text{ Pa}\cdot\text{m}^{-1}$, correspondant à des vitesses de pompage d'Ekman de l'ordre de $3 \text{ m}\cdot\text{jour}^{-1}$ pour Hawaii et $4 \text{ m}\cdot\text{jour}^{-1}$ pour le Cap Vert. Elles engendrent des tourbillons cycloniques et anticycloniques au nord et au sud du sillage de chaque île. La réponse de la circulation océanique est étudié à l'aide d'une simple balance de Sverdrup. Deux gyres océaniques de Sverdrup se forment à l'ouest de l'île d'Hawaii, et s'étendent jusqu'au bord ouest du Pacifique. Un transport zonal vers l'est en résulte, confiné entre 19°N et 20°N . À l'est de 170°W , l'expression de ce transport coïncide avec le Hawaiian Lee Counter Current. La formation de gyres similaires est prévue dans l'Atlantique, mais n'a pas encore été observée. Les résultats suggèrent que les structures du vent à méso-échelle se formant dans le sillage d'îles montagneuses doivent être incluses dans le forçage des modèles de circulation océanique.

Introduction

Oceanic islands with high topography drastically affect both the atmospheric and oceanic flows. Sharp horizontal wind shear lines often form on the edges of the island wake (**Figure 1a**), resulting in rapid variations of the Ekman transport in the ocean, strong upwelling and downwelling, and spin-up of mesoscale eddies (Barton, 2001). The input of vorticity from the wind stress to the ocean and the blocking effect of the island ridge on the impinging currents affect the large-scale oceanic circulation. These processes are enhanced when the wind is steady and capped by an atmospheric inversion layer, as in the trade-wind belt.

Using National Aeronautics and Space Administration scatterometer (NSCAT) measurements at 25 km resolution, mean sea surface wind fields were computed in the vicinity of various islands (Chavanne et al., 2000; Hermes, 2000). Some of the most pronounced interactions with the atmospheric flow are found for Hawaii in the Pacific Ocean and Cabo Verde in the Atlantic Ocean. The Hawaiian archipelago presents a 600-km-

long series of high vertical obstacles to the wind. It is situated south of the atmospheric North Pacific High, between 19°N and 22°N , in steady trade winds of $6 \text{ m}\cdot\text{s}^{-1}$, with an inversion typically at 2000 m altitude (Chen and Feng, 1995), thus below

Received 24 December 2001. Accepted 18 March 2002.

C. Chavanne,¹ P. Flament,² and A. Bentamy. Département d'Océanographie Spatiale, Institut Français de Recherche pour l'Exploitation de la Mer, 29280 Plouzané, France.

R. Lumpkin. Department of Oceanography, Florida State University, Tallahassee, FL 32306, U.S.A.

B. Dousset. Hawaii Institute of Geophysics and Planetology, University of Hawaii, Honolulu, HI 96822, U.S.A.

¹Corresponding author. Present address: Department of Oceanography, School of Ocean and Earth Science and Technology, University of Hawaii, Honolulu, HI 96822, U.S.A. (e-mail: cedric@hawaii.edu).

²Present address: Department of Oceanography, School of Ocean and Earth Science and Technology, University of Hawaii, Honolulu, HI 96822, U.S.A.

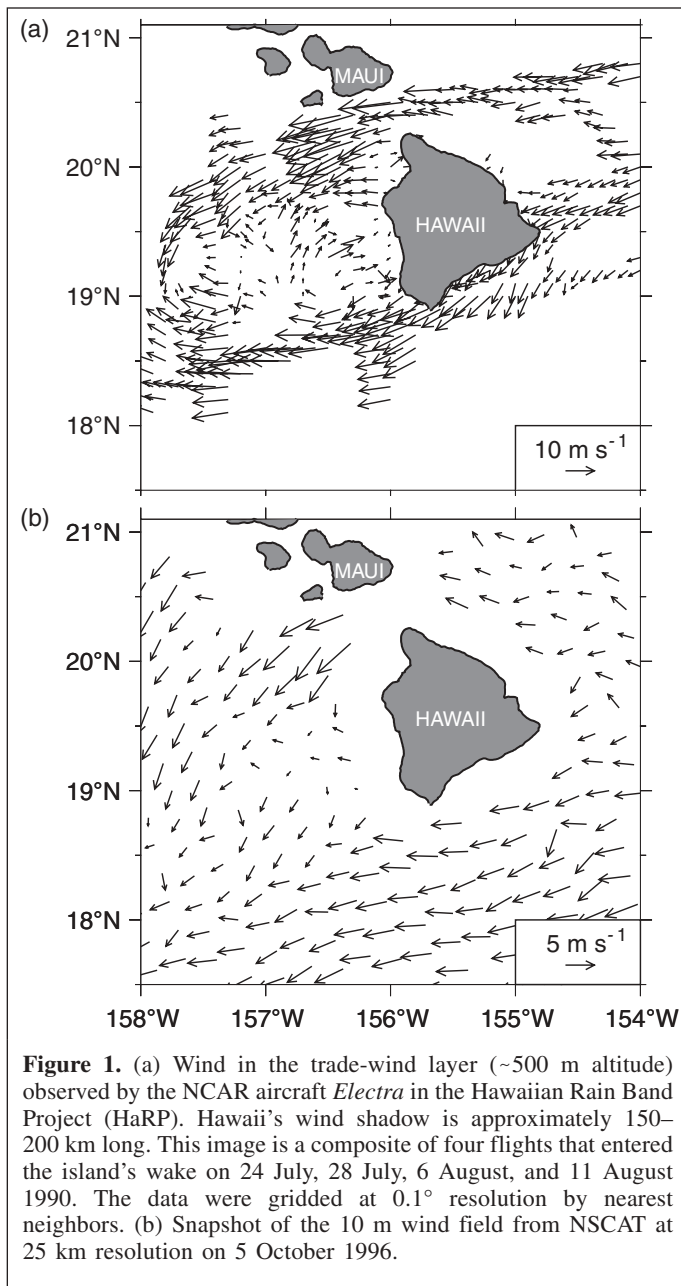


Figure 1. (a) Wind in the trade-wind layer (~500 m altitude) observed by the NCAR aircraft *Electra* in the Hawaiian Rain Band Project (HaRP). Hawaii's wind shadow is approximately 150–200 km long. This image is a composite of four flights that entered the island's wake on 24 July, 28 July, 6 August, and 11 August 1990. The data were gridded at 0.1° resolution by nearest neighbors. (b) Snapshot of the 10 m wind field from NSCAT at 25 km resolution on 5 October 1996.

the highest summits (3000–4200 m). The Cabo Verde archipelago is situated between 15°N and 17°N , 500 km west of the African coast, in strong and steady trade winds of $8 \text{ m}\cdot\text{s}^{-1}$, generated by the Azores High – Saharan Low system. The highest islands (1500–2800 m) also are above the inversion layer, which typically lies between 500 and 700 m.

The paper presents and discusses the impact of wind stress variations induced by these islands on the ocean circulation, using simple Ekman and Sverdrup models.

Data

The available NSCAT wind data span the 9 month period from 9 September 1996 to 29 June 1997, when the advanced

Earth observing satellite (ADEOS) failed. Although less than an annual cycle, this period is sufficient to study processes in the rather steady trade-wind belt. Data are taken from the high-resolution merged geophysical data product (HR-MGDR) level of the NSCAT, derived from the standard level 1.5 (Dunbar, 1997), which provides four wind vector ambiguities retrieved from backscatter measurements collocated in $25 \times 25 \text{ km}$ cells. The solution with the greatest likelihood was retained.

Scatterometers, while measuring the roughness of the ocean surface, are calibrated against the equivalent 10-m neutral wind, rather than wind stress (τ), which is difficult to measure directly. The wind stress is derived from the bulk formula $\tau = \rho_a C_D U_{10}^2$, where C_D is the drag coefficient for neutral stability conditions (Smith, 1988), U_{10} is the wind speed at an altitude of 10 m, and $\rho_a = 1.225 \text{ kg}\cdot\text{m}^{-3}$. We ignore the effects of air–sea temperature differences on the wind stress which may be important, especially in areas of strong diurnal warming (Flament et al., 1994). The error introduced by this approximation is discussed at the end of the section.

The wind stress was computed for each satellite pass (as a quadratic function of wind speed, it cannot be computed from the average). The curl was calculated from a bilinear regression of the stress components in four-adjacent-point cells, as a compromise between spatial resolution and regression sample size. The divergence of the 10-m wind was calculated similarly.

The individual curl and divergence estimates were then remapped to a fixed 0.25° grid by nearest neighbors, and the median of all observations over the NSCAT period was taken at each grid point. The robust median operator was chosen to avoid bias by extreme phenomena such as fronts or hurricanes.

The 25 km resolution allows us to resolve some of the complex features of the wind field in the lee of the islands. **Figure 1a** shows a composite picture of the wind field around the island of Hawaii by the *Electra* aircraft from the National Center for Atmospheric Research (NCAR) at a very high spatial resolution, and **Figure 1b** shows a snapshot of the wind field as observed by NSCAT on a different day but under a similar trade-winds regime. The acceleration of the wind on the edges of the island of Hawaii and the weakening in its lee are well resolved. The sharp shear lines and the lee eddies present in the aircraft observations (Smith and Grubišić, 1993), however, are not fully resolved by the scatterometer.

NSCAT has good temporal coverage of nearly one observation per day for each grid point on the ocean surface, except near the islands because of the land masks. Grid point values for which the total number of observations for the entire period was less than 170 were dismissed in the Sverdrup flow computations.

Sea surface temperatures (SST) were also obtained at 1-km resolution from the National Oceanic and Atmospheric Administration (NOAA) advanced very high resolution radiometer (AVHRR). A total of 619 images were collected during the NSCAT period. The multi-channel sea surface temperature algorithm of McClain et al. (1985) was used, with the most recent coefficients released by NOAA. The cloud-detection procedure of Dousset et al. (1998) was used to reject

cloudy pixels. **Figure 2** shows a progressive increase of SST westward of the Hawaiian islands. The gradient is $\sim 8.10^{-7} \text{ K}\cdot\text{m}^{-1}$. The temperature of a 2000-m thick trade-wind layer, initially in thermal equilibrium with the ocean, and subsequently advected over warmer water, would lag behind the SST by at most 1.5 K, assuming that surface sensible heat flux is acting alone. This corresponds to a $\sim 10\%$ underestimate on the drag coefficient for trade winds of $\sim 5 \text{ m}\cdot\text{s}^{-1}$ and $\sim 4\%$ for trade winds of $\sim 10 \text{ m}\cdot\text{s}^{-1}$ (Smith, 1988). Lacking independent estimates of air temperature, however, a correction for this effect cannot be performed.

To investigate the effect of surface wind divergence on the lower atmosphere, the frequency of cloud occurrence was computed for each pixel (**Figure 3**) using a cloud-detection algorithm based on a threshold of 15°C on channel 4 ($10.5 \mu\text{m}$); this simple algorithm is sufficient to discriminate between small trade winds, convective clouds, and the ocean background.

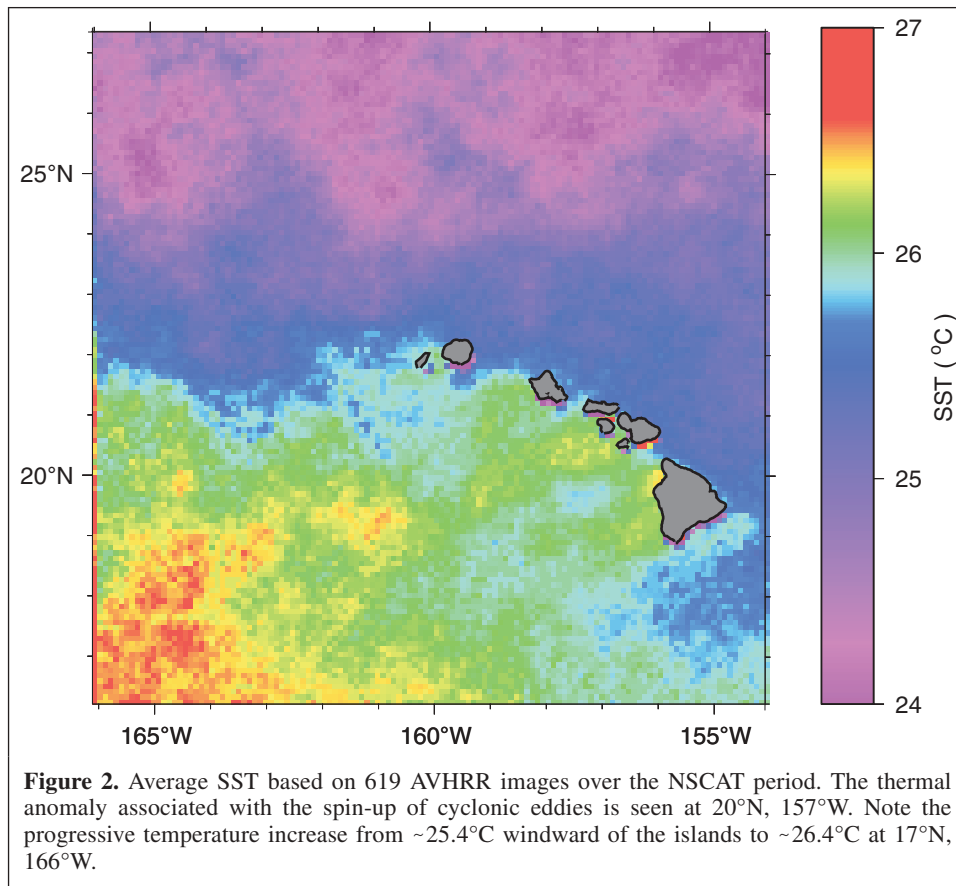
Observations

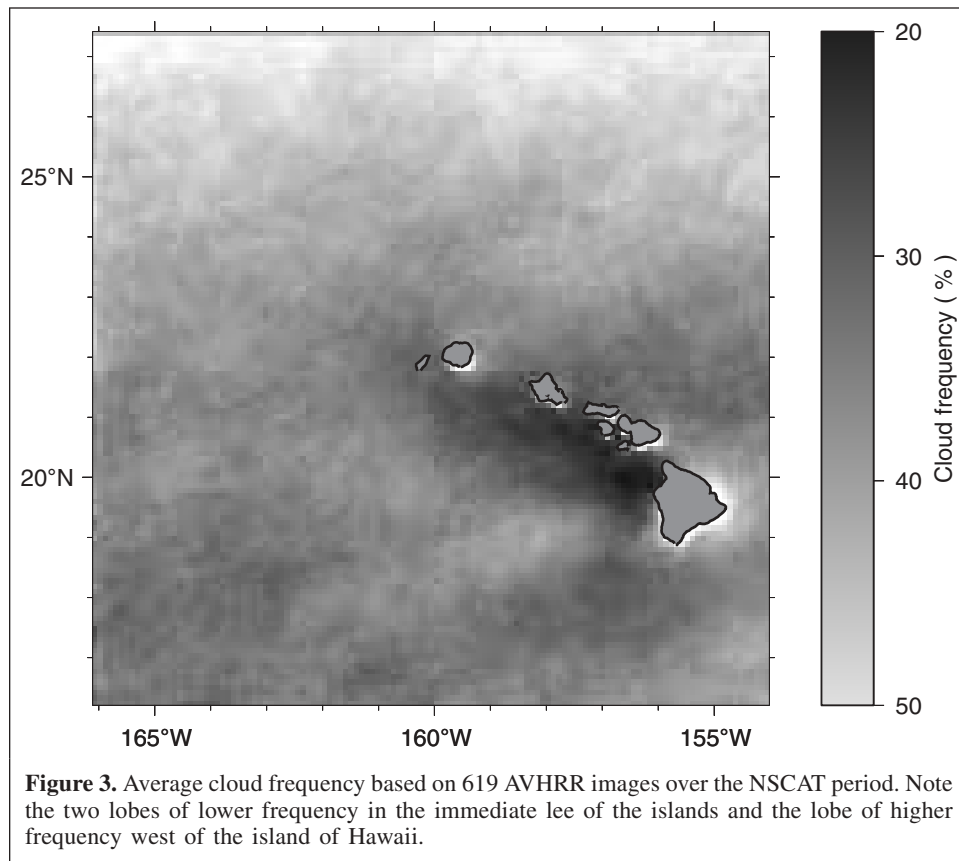
Both the Hawaiian and Cabo Verde archipelagos display similar features in their average wind field. The islands act as barriers to the trade winds, which are confined below the inversion and constrained to flow around the topography. Shadow zones of weak winds are observed in the lee of the islands, separated from lateral bands of accelerated winds

(**Figures 4a, 5a**). This is consistent with the snapshots of **Figure 1**, indicating that the trade-wind regime dominates.

Wind divergence is in phase with wind speed, displaying a pattern of convergence over the shadow zones and divergence within the accelerated jets (**Figures 4b, 5b**), with extrema of the order of f , the Coriolis parameter. Cloud frequency displays a pattern similar to that of wind divergence (**Figures 3, 4b**). Two lobes of cloud frequency lower than 28% extend northwestward and southwestward from the island of Hawaii, with a lobe of cloud frequency higher than 40% between them. Divergence, hence subsidence, is correlated with lower cloud frequency, whereas convergence, hence convection, is correlated with higher cloud frequency. The lower cloud frequency and weaker wind in the immediate lee of the islands result in a progressive downstream increase of SST (**Figure 2**), the incoming radiation flux being enhanced and the sensible and latent heat fluxes reduced.

Wind stress curl is out of phase with wind divergence. There is a dipole of positive curl on the northern side and negative curl on the southern side of the lee of each major island (**Figures 4c, 5c**) associated with the shear lines. The case of Cabo Verde is spectacular. Five dipoles can be distinguished, extending five or six island diameters downstream, and reaching extrema of -10^{-6} and $2.10^{-6} \text{ Pa}\cdot\text{m}^{-1}$. For the Hawaiian archipelago, there are three dipoles associated with the islands of Hawaii, Maui, and Oahu and a less evident one for the island of Kauai. The curl reaches extrema of -2.10^{-6} and $3.10^{-6} \text{ Pa}\cdot\text{m}^{-1}$. These patterns





tend to decay rapidly away from the islands, except for the anticyclonic curl south of the island of Hawaii which extends at least four island diameters downstream. These patterns are similar to those observed by Xie (2001) with monthly averaged QuikSCAT data. The 9-month average suggests that the wind stress curl dipoles associated with each major island are steady features, as sketched in **Figure 6**.

The broad dipole pattern present over the whole Hawaiian archipelago in various wind climatologies, such as those of Hellerman and Rosenstein (Hellerman and Rosenstein, 1983), the European Centre for Medium-Range Weather Forecasts (ECMWF), and objectively mapped NSCAT measurements at 1° resolution (Archer et al., 2000) (**Figure 7a**), is an artifact resulting from low-pass filtering the actual smaller scale features. No such dipole is even observed over Cabo Verde in the 1° resolution field (**Figure 9a**). Caution must therefore be taken when using coarse-resolution wind fields in the presence of high-topography islands.

Implications for ocean circulation

Ekman pumping and eddies

The wind stress variations in the lee of the Hawaiian and Cabo Verde islands drive divergent and convergent Ekman transports in the upper layer of the ocean which must be compensated by vertical water motions.

The upwelling and downwelling velocity is proportional to the wind stress curl, $w = (1/\rho_0) \text{curl}(\bar{\tau}/f)$, where $\rho_0 = 1025 \text{ kg/m}^3$. The value of w reaches magnitudes of 3 m-day^{-1} for Hawaii and 4 m-day^{-1} for Cabo Verde, based on the 9-month mean wind stress curl. Instantaneous pumping velocities may be larger. Shoaling and deepening of the thermocline result in cyclonic and anticyclonic geostrophic eddies (**Figure 6**). This agrees with observations that intense cyclonic and anticyclonic eddies dominate the circulation west of the Hawaiian islands (Patzert, 1969; Lumpkin, 1998). These eddies form in the immediate lee of the islands, the most energetic ones originating west of the island of Hawaii, and drift westward after spin-up. Cyclonic lee eddies appear in the area of strong positive curl, and anticyclonic eddies form in the area of strong negative curl and may be superimposed on anticyclonic eddies generated by hydrodynamic instabilities of the North Equatorial Current (Flament et al., 2001). The upwelling associated with the spin-up of the cyclonic eddies yields a persistent thermal anomaly, seen at 20°N, 157°W in **Figure 2**.

Sverdrup flow

The vorticity input to the ocean by the wind stress curl drives a depth-integrated meridional transport, $V = \int_{-\infty}^0 v dz$, in Sverdrup balance (Sverdrup, 1947):

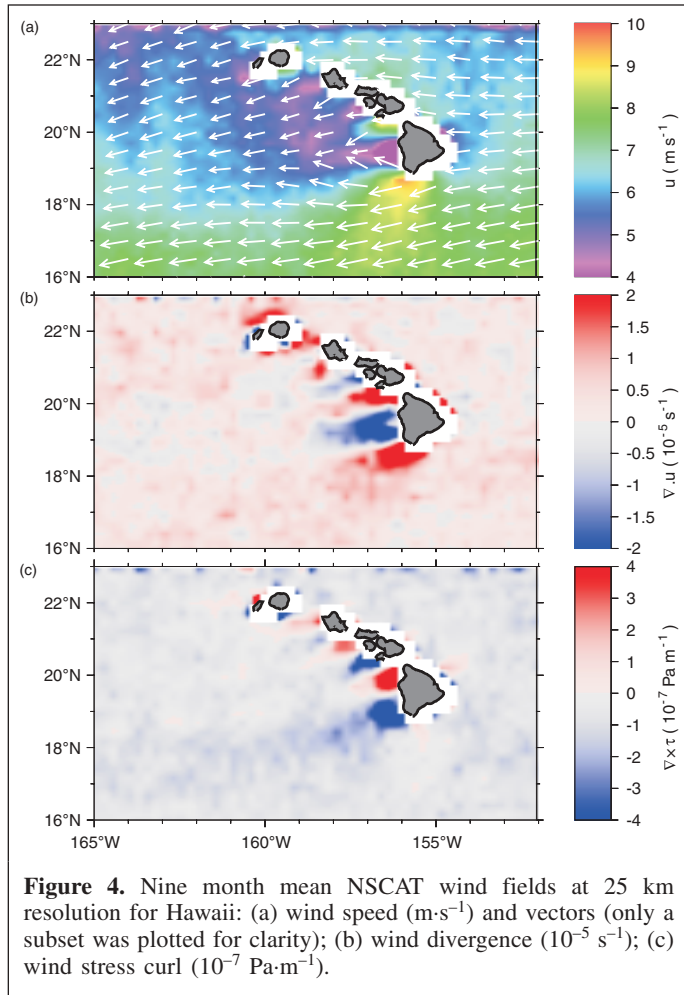


Figure 4. Nine month mean NSCAT wind fields at 25 km resolution for Hawaii: (a) wind speed ($\text{m}\cdot\text{s}^{-1}$) and vectors (only a subset was plotted for clarity); (b) wind divergence (10^{-5} s^{-1}); (c) wind stress curl ($10^{-7} \text{ Pa}\cdot\text{m}^{-1}$).

$$\beta V = \frac{1}{\rho_0} \text{curl}(\bar{\tau}) \quad (1)$$

The Sverdrup transport being horizontally non-divergent, a stream function ψ such that $\partial\psi/\partial x = V$ and $\partial\psi/\partial y = -U$ can be defined, yielding

$$\psi(x, y) = \frac{1}{\beta\rho_0} \int_{x_0(y)}^x \text{curl}(\bar{\tau})(x', y) dx' \quad (2)$$

where $x_0(y)$ is the eastern boundary, and $\psi(x_0, y) = c^{\text{st}} = 0$ to satisfy the no normal flow condition. In the absence of islands, the integral can be carried from the eastern boundary to the western boundary of the ocean basin. The situation is complicated in the presence of islands. The reader is referred to Godfrey (1989) and Firing et al. (1999) for a thorough treatment of this case. The present paper is focussed on island-induced wind effects on the ocean circulation, not on the blocking effect of the islands on the large-scale currents. Both interior flow solutions can be superimposed at the linear Sverdrup approximation. We will thus look at the Sverdrup flow anomalies induced by the wind stress curl anomalies.

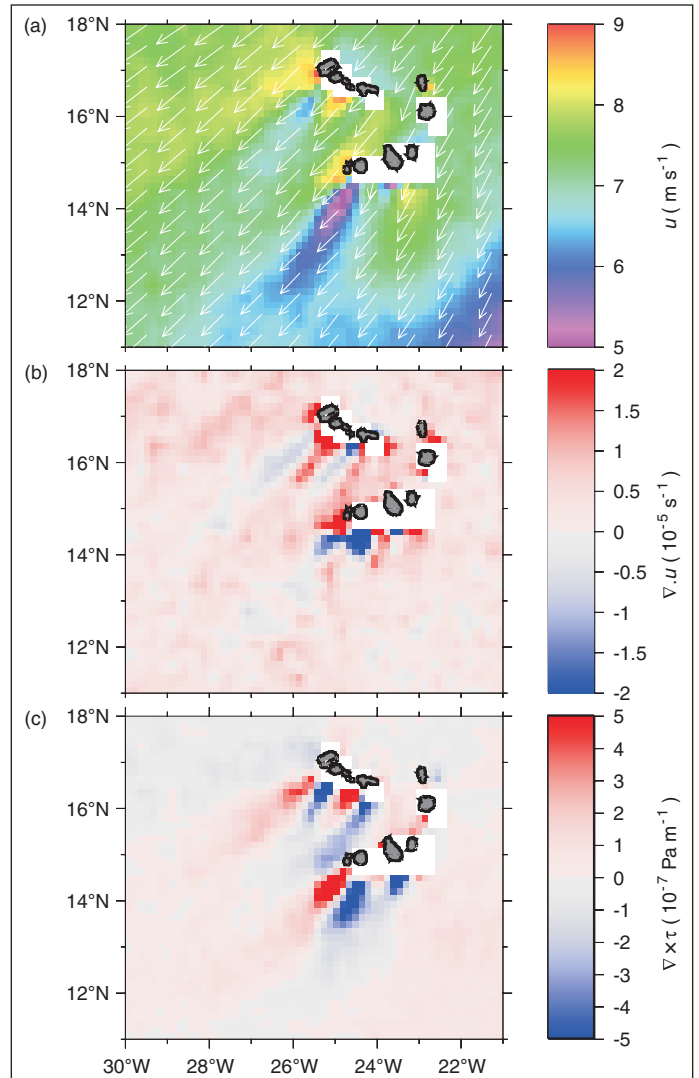


Figure 5. Nine month mean NSCAT wind fields at 25 km resolution for Cabo Verde: (a) wind speed ($\text{m}\cdot\text{s}^{-1}$) and vectors (only a subset has been plotted for clarity); (b) wind divergence (10^{-5} s^{-1}); (c) wind stress curl ($10^{-7} \text{ Pa}\cdot\text{m}^{-1}$).

Assuming a current profile of the form $u = u_0 e^{-z/z_0}$ with a typical thermocline depth $z_0 = 400 \text{ m}$, the surface currents associated with the Sverdrup transport will roughly scale as $u_0 = U/z_0$.

A large-scale Sverdrup transport stream function was first computed from the global, objectively mapped 1° resolution NSCAT wind stress curl (Archer et al., 2000) (Figures 7a–7c). The subtropical gyre is distorted by the curl dipole present over the Hawaiian islands, yielding a weak $\sim 3 \text{ cm}\cdot\text{s}^{-1}$ eastward countercurrent at about 20°N west of Hawaii, in qualitative agreement with numerical simulations based on National Centers for Environmental Prediction (NCEP) and ECMWF reanalyses (Xie, 2001). This countercurrent, however, may be an artifact of the single broad dipole present in the 1° resolution data. A high-resolution curl field was therefore constructed as follows to remove the artificial dipole. The low-resolution field was replaced by a bilinear interpolation from the boundaries over the domain ($170\text{--}150^\circ\text{W}$, $15\text{--}25^\circ\text{N}$). The high-resolution

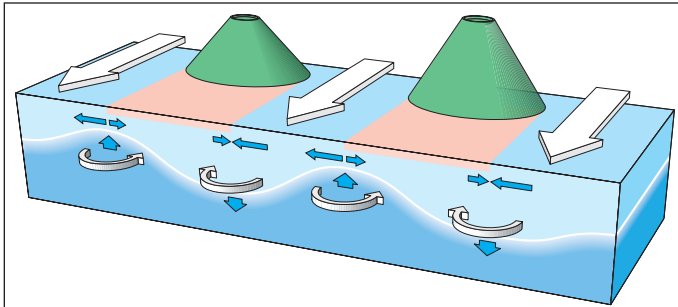


Figure 6. Conceptual diagram showing Ekman pumping in the lee of islands. The large white arrows represent intensified winds in the channels, yielding cooler surface temperatures; in the calm lee, surface temperatures are warmer. These wind speed variations induce divergent and convergent surface currents, which in turn lift or depress the thermocline, forming cyclonic and anticyclonic eddies.

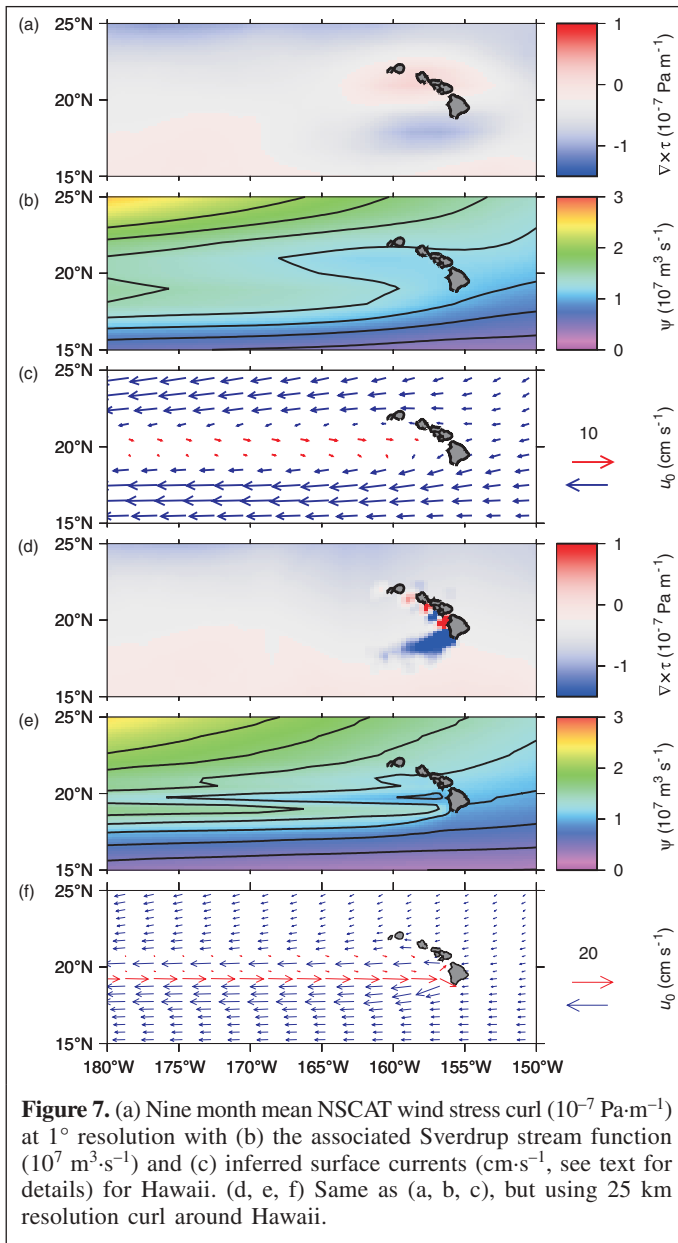


Figure 7. (a) Nine month mean NSCAT wind stress curl ($10^{-7} \text{ Pa}\cdot\text{m}^{-1}$) at 1° resolution with (b) the associated Sverdrup stream function ($10^7 \text{ m}^3\cdot\text{s}^{-1}$) and (c) inferred surface currents ($\text{cm}\cdot\text{s}^{-1}$, see text for details) for Hawaii. (d, e, f) Same as (a, b, c), but using 25 km resolution curl around Hawaii.

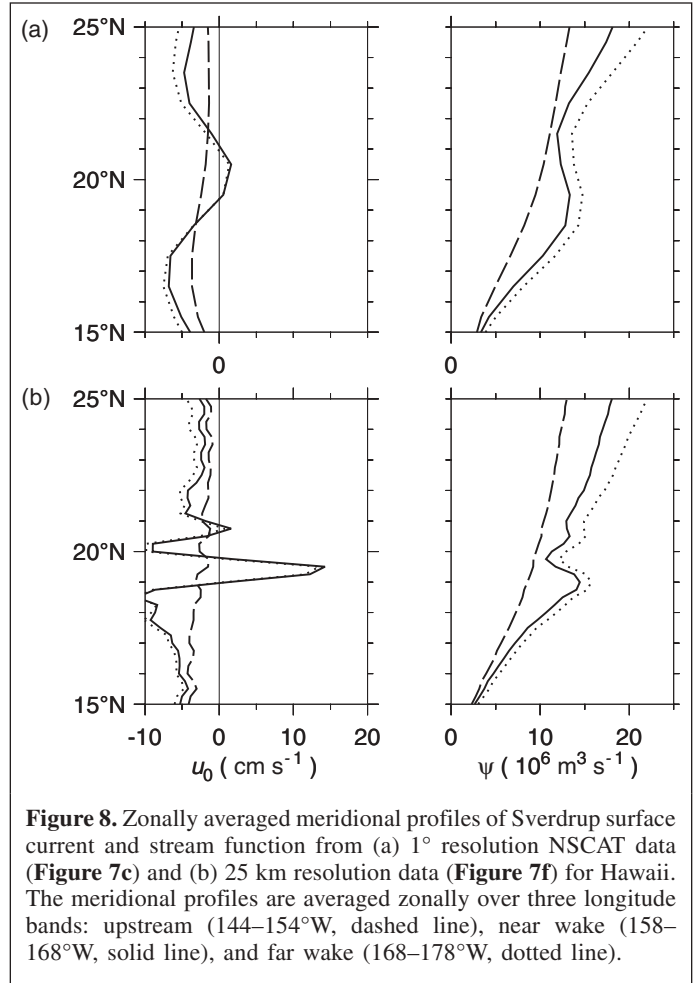
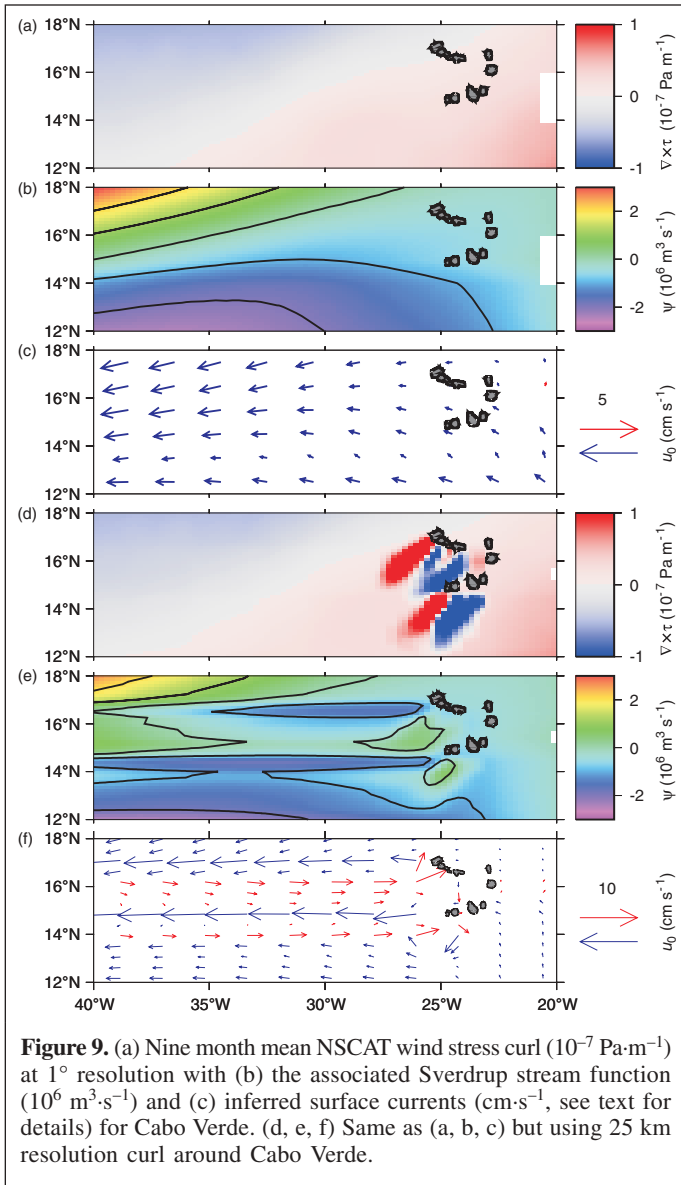


Figure 8. Zonally averaged meridional profiles of Sverdrup surface current and stream function from (a) 1° resolution NSCAT data (Figure 7c) and (b) 25 km resolution data (Figure 7f) for Hawaii. The meridional profiles are averaged zonally over three longitude bands: upstream ($144\text{--}154^\circ\text{W}$, dashed line), near wake ($158\text{--}168^\circ\text{W}$, solid line), and far wake ($168\text{--}178^\circ\text{W}$, dotted line).

curl including the actual multiple dipoles was then inserted in this domain, with values differing by less than $10^{-7} \text{ Pa}\cdot\text{m}^{-1}$ from the low-resolution curl being filtered out as measurement noise. This filtering is necessary because the Sverdrup transport is a second-order derivative of the wind stress, and therefore extremely sensitive to noise.

The resulting stream function and associated surface currents are shown in Figures 7e and 7f and their zonal averages in Figure 8. The eastward countercurrent appears stronger ($10\text{--}15 \text{ cm}\cdot\text{s}^{-1}$ at the surface) and narrower than with the 1° resolution data. It is centered at 19.5°N and is due to the dipole of the island of Hawaii. Another smaller countercurrent appears at 20.5°N , due to the dipole of the island of Maui. Two accelerated westward jets appear north and south of the island of Hawaii as a result of the elongated counter-rotating Sverdrup gyres spun up by the wind stress curl dipoles.

A similar treatment was applied to the case of the Cabo Verde islands. The resulting stream function and associated surface currents are shown in Figures 9e and 9f and their zonal averages in Figure 10. There may be two countercurrents west of the islands, a broad one centered at 16°N and a narrow one centered at 14°N . They are weaker ($3\text{--}5 \text{ cm}\cdot\text{s}^{-1}$ at the surface) than the countercurrent of Hawaii because the curl dipoles have a more pronounced southwest–northeast orientation, hence

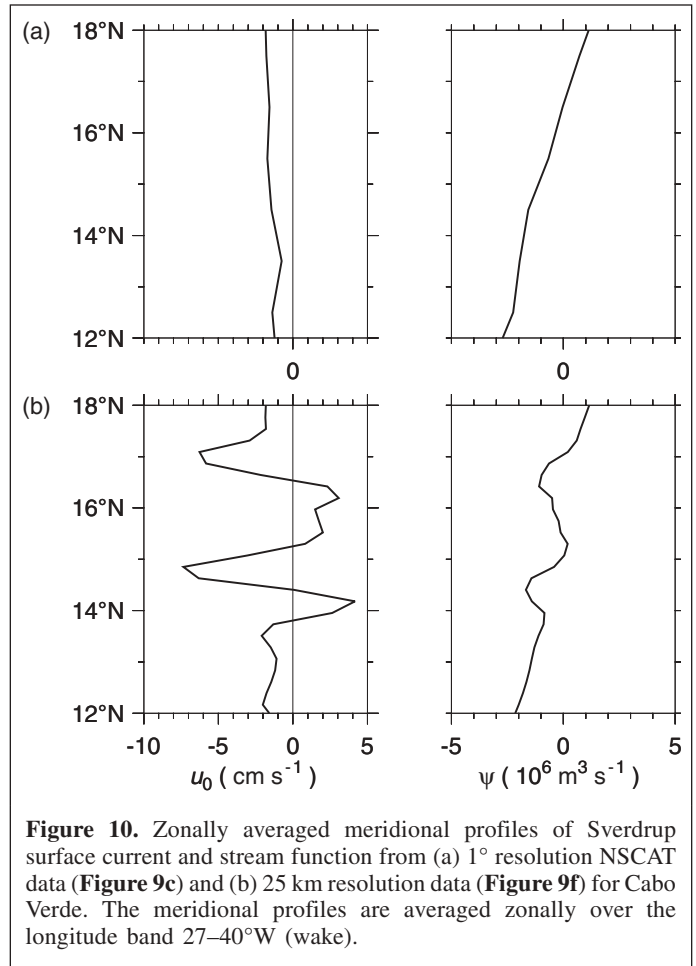


roughly cancelling themselves in the zonal integral of Equation (2); however, localized Sverdrup gyres are formed in the immediate vicinity of the islands.

Discussion

A goal of this paper was to show how high-resolution scatterometers reveal wind field structures induced by high-topography oceanic islands. The cases of Hawaii and Cabo Verde were presented, using NSCAT winds at 25 km resolution. In both archipelagos the islands have a profound impact on the mean wind field, featuring wakes of weak winds, flanked by accelerated winds. The resulting wind stress curl reaches magnitudes of $10^{-6} \text{ Pa}\cdot\text{m}^{-1}$, drastically affecting the ocean circulation.

The complex pattern of mean surface ocean currents around Hawaii, as measured by drifting buoys, is shown in **Figure 11**



(cf. Lumpkin and Flament, 2001). A zonal eastward countercurrent of $\sim 10 \text{ cm}\cdot\text{s}^{-1}$, the Hawaiian Lee Counter Current (HLCC; Flament et al., 1998), extends from 168°W to 156°W at 19.5°N and dominates the mean flow in the lee of the islands. The HLCC and the acceleration of the North Equatorial Current (NEC) south of the island of Hawaii correspond fairly well with the Sverdrup transport computed from the NSCAT measurements (**Figure 7f**). The main differences are that the observed HLCC extends only to 168°W , whereas the Sverdrup countercurrent is predicted to extend to the western boundary of the Pacific Ocean (not shown), and the second Sverdrup countercurrent at 20.5°N and the accelerated westward jet at 20°N have not yet been observed. It is not known if multiple alternating currents actually exist, prompting further current observations.

As shown by Qiu et al. (1997) and Firing et al. (1999), the net effect of the presence of the islands in the NEC is to induce two accelerated jets on their southern and northern ends, joining the background westward flow. These are linear results and can therefore be superimposed on the linear Sverdrup flow induced by the wind anomalies. The similarity between the computed Sverdrup transport and the observations of surface currents suggests that stress curl anomalies alone can explain the existence of the HLCC, even without the blocking effect of the

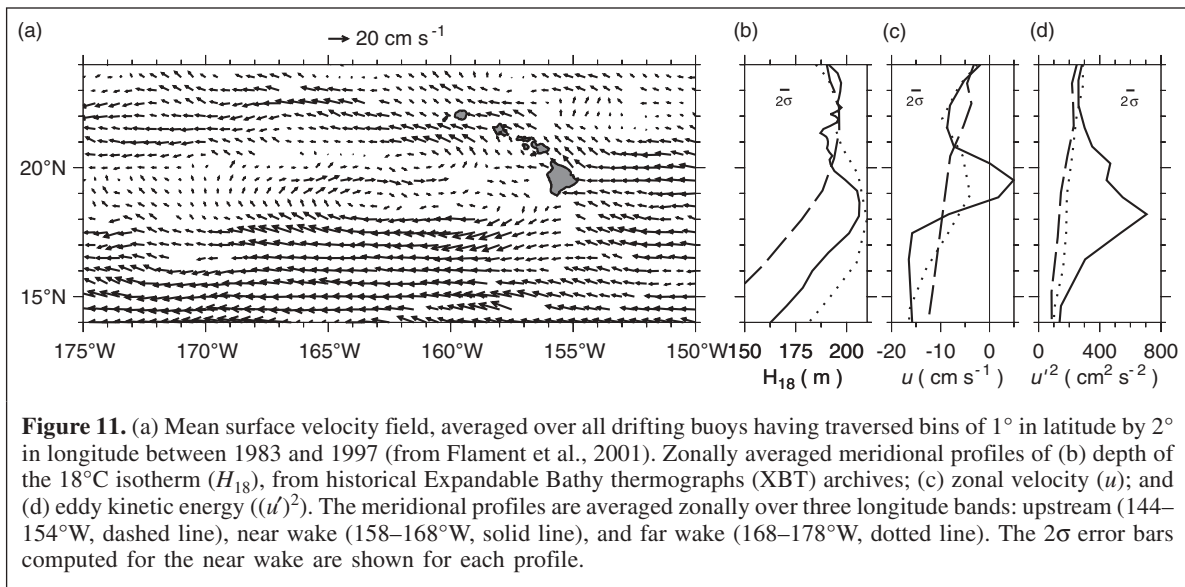


Figure 11. (a) Mean surface velocity field, averaged over all drifting buoys having traversed bins of 1° in latitude by 2° in longitude between 1983 and 1997 (from Flament et al., 2001). Zonally averaged meridional profiles of (b) depth of the 18°C isotherm (H_{18}), from historical Expandable Bathy thermographs (XBT) archives; (c) zonal velocity (u); and (d) eddy kinetic energy ($(u')^2$). The meridional profiles are averaged zonally over three longitude bands: upstream ($144\text{--}154^\circ\text{W}$, dashed line), near wake ($158\text{--}168^\circ\text{W}$, solid line), and far wake ($168\text{--}178^\circ\text{W}$, dotted line). The 2σ error bars computed for the near wake are shown for each profile.

islands in the oceanic flow. The wind anomaly is so strong that it can drive an eastward transport, against the general westward NEC. The presence of islands in fact enhances the eastward HLCC, since they block the westward flow of the NEC. The wind stress curl anomalies also contribute to the acceleration of the NEC as it passes south of the island of Hawaii.

Features similar to the HLCC, though weaker, are predicted in the lee of Cabo Verde. Observational surveys in the lee of this archipelago, and of numerous other islands around the world, are required to confirm that lee countercurrents are a general property of high-topography oceanic islands. The advent of 12.5 km resolution QuikSCAT data promises further improvements in the study of high-topography islands or coastline wind wakes and their influence on the general ocean circulation.

Acknowledgments

This work was supported by an undergraduate fellowship from the Institut Français de Recherche pour l'Exploitation de la Mer (IFREMER) and by the host institutions of the authors. Juliet Hermes processed the Cabo Verde data. Io Flament was responsible for the cloud statistics of **Figure 3**. Julie Deshayes and Adrien Desoria prepared the figures, using the plotting package *gri* by Dan Kelley. The NSCAT data were provided by the Centre ERS d'Archivage et de Traitement (CERSAT) at IFREMER, based on level 2b data released by the Physical Oceanography Distributed Active Archive Center (PO-DAAC) at the Jet Propulsion Laboratory. Eric Firing, Bo Qiu, Shang-Ping Xie, and Zuojun Yu are acknowledged for helpful discussions. School of Ocean and Earth Science and Technology, University of Hawaii, Contribution 5962, and Joint Institute of Marine and Atmospheric Research Contribution 02-341.

References

- Archer, O., Bentamy, A., Firing, J., Flament, P., Harscoat, V., Loubrieu, F., Maroni, C., Piolle, J., Pouliquen, S., Quilfen, Y., and Sawyer, M. 2000. Mean surface wind fields from the ERS-AMI and ADEOS-NSCAT microwave scatterometers, 1991–2000. Technical report WOCMWF2, Département d'Océanographie Spatiale, Institut Français de Recherche pour l'Exploitation de la Mer (IFREMER), Plouzané, France.
- Barton, E. 2001. Island wakes. In *Encyclopedia of ocean sciences*. Edited by J. Steele, K. Turekian, and S. Thorpe. Academic Press, New York, Vol. 3, pp. 1397–1403.
- Chavanne, C., Hermes, J., and Flament, P. 2000. Mesoscale wind field in the lee of strong topographic features. *Cersat News*, Vol. 11, pp. 9–10.
- Chen, Y.-L., and Feng, J. 1995. The influences of inversion height on precipitation and airflow over the island of Hawaii. *Monthly Weather Review*, Vol. 123, pp. 1660–1676.
- Doussat, B., Firing, J., Flament, P., Jackson, H., Lumpkin, C., Maroni, C., Nacini, E., Poulain, P., Pouliquen, S., Sawyer, M., and Young, D. 1998. Adriatic sea surface temperature images from the NOAA-AVHRR 1995. CD-ROM, <<http://satftp.soest.hawaii.edu/adriatic/>>, Département d'Océanographie Spatiale, Institut Français de Recherche pour l'Exploitation de la Mer (IFREMER), Plouzané, France.
- Dunbar, S. 1997. High-resolution merged geophysical data product, NASA scatterometer, user's guide. Technical Report 1.1, Jet Propulsion Laboratory, California Institute of Technology, Pasadena, Calif.
- Firing, E., Qiu, B., and Miao, W. 1999. Time-dependent island rule and its application to the time-varying North Hawaiian Ridge current. *Journal of Physical Oceanography*, Vol. 29, pp. 2671–2688.
- Flament, P., Firing, J., Sawyer, M., and Trefois, C. 1994. Amplitude and horizontal structure of a large diurnal sea surface warming event during the Coastal Ocean Dynamics Experiment. *Journal of Physical Oceanography*, Vol. 24, pp. 123–139.
- Flament, P., Kennan, S., Lumpkin, R., Sawyer, M., and Stroup, E. 1998. *The ocean atlas of Hawaii*. University of Hawaii Press, Honolulu, Hawaii, pp. 82–86.

- Flament, P., Lumpkin, R., Tournadre, J., and Armi, L. 2001. Vortex pairing in an unstable anticyclonic shear flow: discrete subharmonics of one pendulum day. *Journal of Fluid Mechanics*, Vol. 440, pp. 401–409.
- Godfrey, J. 1989. A Sverdrup model of the depth-integrated flow for the world ocean allowing for island circulations. *Geophysical and Astrophysical Fluid Dynamics*, Vol. 45, pp. 89–112.
- Hellerman, S., and Rosenstein, M. 1983. Normal monthly wind stress over the world ocean with error estimates. *Journal of Physical Oceanography*, Vol. 13, pp. 1093–1104.
- Hermes, J. 2000. Small scale variability of surface wind in the lee of strong topographic features, and its influence on ocean circulation. M.Sc. thesis, School of Ocean Sciences, University of Wales, Bangor, U.K.
- Lumpkin, C. 1988. Eddies and currents of the Hawaiian Islands. Ph.D. dissertation, School of Ocean and Earth Sciences and Technology, University of Hawaii at Manoa, Manoa, Hawaii.
- Lumpkin, R., and Flament, P. 2001. Lagrangian statistics in the central North Pacific. *Journal of Marine Systems*, Vol. 29, pp. 141–155.
- McClain, E.P., Pichel, W.G., and Walton, C.C. 1985. Comparative performance of AVHRR-based multichannel sea surface temperatures. *Journal of Geophysical Research*, Vol. 90, pp. 11 587 – 11 601.
- Patzert, W.C. 1969. Eddies in Hawaiian waters. Technical Report 69-8, Hawaiian Institute of Geophysics, University of Hawaii at Manoa, Honolulu, Hawaii.
- Qiu, B., Koh, D.A., Lumpkin, C., and Flament, P. 1997. Existence and formation mechanism for the North Hawaiian Ridge Current. *Journal of Physical Oceanography*, Vol. 27, pp. 431–444.
- Smith, S. 1988. Coefficients for sea surface wind stress, heat flux and wind profile as a function of wind speed and temperature. *Journal of Geophysical Research*, Vol. 93, pp. 15 467 – 15 472.
- Smith, R.B., and Grubišić, V. 1993. Aerial observations of Hawaii's Wake. *Journal of the Atmospheric Sciences*, Vol. 50, pp. 3728–3750.
- Sverdrup, H.U. 1947. Wind-driven currents in a baroclinic ocean; with application to the equatorial currents of the eastern Pacific. *Proceedings of the National Academy of Sciences of the United States of America*, Vol. 33, pp. 318–326.
- Xie, S.-P. 2001. Far-reaching effects of the Hawaiian islands on the Pacific ocean–atmosphere. *Science (Washington, D.C.)*, Vol. 292, pp. 1953–2304.